Cold sintering of magnetic $BaFe_{12}O_{19}$ and other ferrites at 300ºC

Sarah Lowum[1]* (sml92@psu.edu), Richard Floyd[1] (richard@richardfloyd.com), Yanglin Zhu[2] (ybz5326@psu.edu), Zhiqiang Mao[2] (zim1@psu.edu), and Jon-Paul Maria[1] (jpm133@psu.edu)

[1]Department of Materials Science and Engineering, The Pennsylvania State University, University Park, Pennsylvania, 16802, USA

[2]Department of Physics, The Pennsylvania State University, University Park, Pennsylvania, 16802, USA

Author Mailing Address:

215 Steidle Building
Pennsylvania State University
University Park, PA 16802

Author ORCiDs:

Sarah Lowum: 0000-0003-0771-2820
Richard Floyd: 0000-0003-3482-4940
Yanglin Zhu: 0000-0002-6692-1406
Zhiqiang Mao: 0000-0002-4920-3293
Jon-Paul Maria: 0000-0003-3604-4761

Abstract

Densification to > 90% at 300ºC is demonstrated in $ZnFe_2O_4$ and $BaFe_{12}O_{19}$ via hydroflux-assisted densification (HAD), a derivative of the cold sintering process employing non-aqueous, flux-based mass transport phases to facilitate densification. Previous attempts to cold sinter these materials with aqueous-based mass transport phases were not as successful. Attempts to densify $NiFe_2O_4$ and $(Ni_{0.5}Zn_{0.5})Fe_2O_4$ only achieved densities around 80%. Magnetic hysteresis measurements of the low-temperature densified $BaFe_{12}O_{19}$ samples produced magnetic saturation values as high as 93 emu/g and coercive fields as high as 1789 Oe, which are comparable to values reported in the literature for this material produced via other processing techniques. Additional techniques are suggested to further optimize the magnetic properties of $BaFe_{12}O_{19}$ densified following the HAD approach.

I. Introduction

Cold sintering, a low-temperature (300ºC or below) densification route for ceramics, has become increasingly studied over the past several years, with suggested applications including dielectrics, ferroelectrics, refractory ceramics, cathode materials, thermoelectrics, and solid electrolytes [1–3]. However, one of the critical ingredients in cold sintering is a secondary phase that drives mass transport and densification in the parent ceramic. Similar to liquid phase sintering, this secondary mass transport phase inherently introduces impurities into the final ceramic, which can degrade the final properties. Electrical properties can be particularly sensitive to grain boundary chemistry and impurity phases and therefore, a post-annealing step is often required for cold-sintered materials to achieve desired electrical properties [4–6]. It has also been shown that mechanical properties can be affected by the cold sintering process, possibly because grain boundaries are not as well bonded in cold-sintered materials or because residual amorphous material exists at the grain boundaries [4, 7]. These issues make it challenging to establish cold sintering as a preferred processing technique for many materials.

One promising application where the benefits of cold sintering have been undervalued is in magnetic materials. Magnetic properties are closely related to the starting material composition and morphology [8, 9], which can be easily controlled and maintained in cold sintering. The remarkably low temperatures of cold sintering circumvent several problems associated with the high temperatures required for traditional sintering, such as grain growth and alteration of defect chemistry. Furthermore, these low temperatures allow for incorporation of metals or polymers during sintering, enabling single-step formation of functional devices. Thirdly, the cold sintering process produces net shape ceramics that conform to the pressing apparatus, providing opportunities to sinter complex geometries (i.e. toroids, plates, mesh) without costly and time-

consuming machining. To date, the authors are unaware of any data on magnetic properties of cold-sintered materials published in the peer-reviewed literature despite the potential advantages of this process.

This work aims to investigate the low-temperature densification of ferrite materials for magnetic applications. Many ferrites possess the cubic spinel structure, including $ZnFe_2O_4$, $NiFe_2O_4$, and $(Ni_{0.5}Zn_{0.5})Fe_2O_4$ discussed in this work and a few others [10–12], although there is a second group of ferrites that have a hexagonal structure and are therefore referred to as the hexaferrites. $BaFe_{12}O_{19}$, or barium hexaferrite, is one such material of particular interest due to its high saturation magnetization, good chemical stability, oxidation and corrosion resistance, and the low cost of its raw materials [13]. These key factors have enabled $BaFe_{12}O_{19}$ to be commonplace in applications such as speakers, magnetic card strips, and magnetic recording.

Sintering of $BaFe_{12}O_{19}$ is typically carried out at temperatures between 900ºC and 1300ºC [8, 14, 15]. Ni and Zn-based ferrites require similarly high sintering temperatures 1000ºC or above [16, 17]. Such high temperatures are often unfavorable because they degrade magnetic properties, cause large grain growth, and prevent incorporation of temperature-sensitive materials, such as polymers or metals [9, 15, 18]. Some investigations into suppressing sintering temperature have been performed, such as adding a secondary glass phase or using an alternative technique like spark plasma sintering, but these methods still require temperatures between 800ºC and 900ºC [9, 15, 19, 20], which is generally too high for the incorporation of polymers or metals.

Cold sintering offers an alternative route to densify these materials at only a few hundred degrees Centigrade. Faouri et al. have studied cold sintering of $BaFe_{12}O_{19}$, demonstrating dense Li_2MoO_4-$BaFe_{12}O_{19}$ composites using water, although only up to 15 mol.% $BaFe_{12}O_{19}$ was incorporated [21]. More work has been done on cold sintering of spinels, however most

demonstrate limited success. Ndayishimiye et al. discuss cold sintering of spinel Fe_3O_4 (magnetite) using both ethylenediaminetetraacetic acid (EDTA) and a 1:1 mixture of choline chloride and malonic acid, however both of these transport phases resulted in porous ceramics with densities around 80% [10]. Kamani et al. attempted to cold sinter $ZnFe_2O_4$ between 280ºC and 350ºC using a transport phase consisting of acetic acid in ethanol, however densities >90% were not achieved unless an additional heat treatment at 750ºC for 6 hours was applied to the samples [11]. Funahashi et al. densified the spinels Ni-Cu-Zn ferrite and NiO-Mn_2O_3 to around 90% using a mixture of metal acetylacetonates acting as chelating complexes. However, these metal acetylacetonates only produced a density of 82% in the spinel $LiNi_{0.5}Mn_{1.5}O_4$ [12].

Recent advances in cold sintering have shown that non-aqueous, flux-based secondary mass transport phases can enable a much wider variety of materials to be densified at temperatures of 300ºC or below in a process termed hydroflux-assisted densification (HAD) [2]. Early materials exploration efforts realized that Fe_2O_3 could be densified to relatively high densities (~90%) using this approach [22]. Following this discovery, the HAD technique was applied to other ferrite materials of more interest in functional applications, as will be discussed in this manuscript.

II. Experimental

Ferrite powders were synthesized from commercial oxide and carbonate powders. For $ZnFe_2O_4$, ZnO (Alfa Aesar, 44263, 99.9%) and Fe_2O_3 (Alfa Aesar, 47247, 99.9%) were mixed in a 1:1 molar ratio and calcined at 1200ºC for 4 hours. The resulting $ZnFe_2O_4$ powder was then ball-milled in methanol for 40 hours. To synthesize $NiFe_2O_4$, NiO (Alfa Aesar, 12359, 99.9%) and Fe_2O_3 were mixed in a 1:1 molar ratio and calcined at 1100ºC for 2 hours. The resulting $NiFe_2O_4$

powder was ball-milled in methanol for 24 hours. The $(Ni_{0.5}Zn_{0.5})Fe_2O_4$ powder was formed by mixing NiO, ZnO, and Fe_2O_3 in a 1:1:2 molar ratio and then calcining the powders at 1100ºC for 2 hours (under flowing O_2). The resulting $(Ni_{0.5}Zn_{0.5})Fe_2O_4$ powder was ball-milled in methanol for 24 hours. $BaFe_{12}O_{19}$ was also synthesized via solid-state reaction. $BaCO_3$ (Sigma-Aldrich, 237108, >99%) and Fe_2O_3 powders were mixed in a 1:6 molar ratio and calcined at 1350ºC for 1 hour. The resulting $BaFe_{12}O_{19}$ powder was ball-milled in methanol for 48 hours. All milled powders were dried in a rotary evaporator to remove the methanol. $ZnFe_2O_4$, $NiFe_2O_4$, and $(Ni_{0.5}Zn_{0.5})Fe_2O_4$ powders were stored in an 80ºC vacuum oven. $BaFe_{12}O_{19}$ powder was stored in a glovebox purged with dry air (<10 ppm H_2O) and connected to a DRI-TRAIN HE-493 recirculation system designed to remove moisture, allowing it to maintain a relative humidity <1%.

For the secondary mass transport phase, a eutectic 51:49 molar ratio of NaOH:KOH (referred to as "NaK") was used. The purchased commercial NaOH (Millipore, SX0590-1, A.C.S. Grade) and KOH (Fisher Scientific, P250-500, A.C.S. Grade) came in the form of pellets, so in order to ease mixing of the ceramic powders with the hydroxides, a hydroxide "powder" was first formed. The commercial NaOH and KOH pellets were dissolved in DI water and then the aqueous solutions were dried in an 80ºC vacuum oven until all of the liquid water had evaporated, leaving behind a crystalline hydroxide precipitate. These precipitates were then crushed into a powder-like form. NaOH and KOH powder used as a transport phase for $ZnFe_2O_4$, $NiFe_2O_4$, and $(Ni_{0.5}Zn_{0.5})Fe_2O_4$ was stored in the 80ºC vacuum oven with those respective powders, while NaOH and KOH used to densify $BaFe_{12}O_{19}$ was stored in the dry glovebox with that respective powder. In certain cases, small quantities of DI water were also added to the ceramic powder formulations using a hypodermic needle.

For $ZnFe_2O_4$, $NiFe_2O_4$, and $(Ni_{0.5}Zn_{0.5})Fe_2O_4$ samples, the ceramic and hydroxide powders were weighed in an ambient lab atmosphere and placed into a FlackTek SpeedMixer™ cup. For $BaFe_{12}O_{19}$ samples, the ceramic and hydroxide powders were weighed in the dry glovebox to avoid any water absorption/adsorption during the weighing process. The powders were placed in a FlackTek SpeedMixer™ cup that was then sealed and removed from the glovebox. All ceramic powder formulations were mixed in a FlackTek SpeedMixer™ (Model DAC 150.1 FVZ). Ceramic powder formulations were then loaded into a tungsten carbide pellet die (called an "armadillo die") that was custom-built to provide corrosion and temperature resistance during cold sintering [2]. The die was heated by a Tempco Mi-plus 400W heater band and temperature was monitored by a thermocouple placed into a hole drilled in the shaft collar. A temperature calibration was performed to determine the difference between the thermocouple reading and the actual temperature of the interior die wall. Temperature was controlled with a Tempco TEC-8450 controller. The heating rate used for the presented experiments was 80ºC/min. Samples were pressed using an automatic, hydraulic-powered press called the sinterometer [23]. Temperature and time for the HAD process were held constant at 300ºC and 30 minutes, respectively, for the presented samples. The pressure applied during densification was 530 MPa, unless otherwise noted.

Sample densities were measured volumetrically and compared against theoretical values ($ZnFe_2O_4$ – 5.21 g/cm^3, $NiFe_2O_4$ – 5.33 g/cm^3, $(Ni_{0.5}Zn_{0.5})Fe_2O_4$ – 5.27 g/cm^3, $BaFe_{12}O_{19}$ – 5.28 g/cm^3). Phase identification was performed via x-ray diffraction (Panalytical Empyrean). Microstructures of fracture surfaces were examined using scanning electron microscopy ($BaFe_{12}O_{19}$ - FEI Apreo, other materials – Zeiss SIGMA). Magnetization was measured using a 7 T SQUID magnetometer (Quantum Design).

III. Results and Discussion

$ZnFe_2O_4$ was densified with 8 vol.% NaK and 8 vol.% H_2O. The resulting compact reached a relative density of 96% at 300ºC. This densification is a notable improvement over attempts to cold sinter $ZnFe_2O_4$ with aqueous-based transport phases, which resulted in a maximum density around 85% at 350ºC [11]. Figure 1(a) presents an SEM image of the microstructure of the $ZnFe_2O_4$ sample densified with NaK, showing minimal porosity and a large bimodal grain size distribution. This result demonstrates initial promise for expanding the HAD process to ferrites. However, applying the same densification conditions to $NiFe_2O_4$ and $(Ni_{0.5}Zn_{0.5})Fe_2O_4$ (8 vol.% NaK and 8 vol.% H_2O) resulted in minimal densification (~75%-80%) and structurally fragile ceramics. Figure 1(b) includes a microstructural image of the cold-sintered $(Ni_{0.5}Zn_{0.5})Fe_2O_4$ confirming the lack of densification, as evidenced by the high degree of open porosity and negligible grain boundary formation. Previous attempts to densify NiO with various aqueous and non-aqueous transport phase have shown minimal success [22, 24]. The slow dissolution kinetics and slow ligand exchange rate of Ni^{2+} ions compared to other transition metal cations have been cited as potential reasons for the increased difficulty to cold sinter this material [25–27].

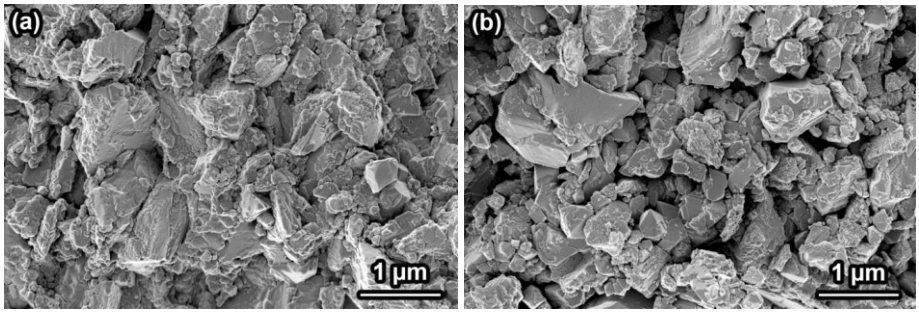

Figure 1 Microstructures of (a) $ZnFe_2O_4$ (96% dense) and (b) $(Ni_{0.5}Zn_{0.5})Fe_2O_4$ (80% dense) following hydroflux-assisted densification using 8 vol.% NaK and 8 vol.% H_2O at 300ºC and 530 MPa for 30 minutes.

Compared to the Ni-containing ferrites, $BaFe_{12}O_{19}$ proved more favorable to hydroflux-assisted densification. Table 1 presents a selection of $BaFe_{12}O_{19}$ samples densified to 89-93% dense at 300ºC with varying volume fractions of transport phase and pressures. Comparing the sample with no added transport phase, which only reached a density of 73%, to any of the samples densified with NaK demonstrates that the addition of NaK clearly enables densification in the $BaFe_{12}O_{19}$ system, given that densities increase 15-20%. Figure 2 presents SEM images of representative microstructures of the samples listed in Table 1. The enhanced densification enabled by NaK is also illustrated by the reduced porosity in the microstructures in Figure 2(b)-(f) as compared to the microstructure of the sample with no added transport phase in Figure 2(a). Further examination of Table 1 reveals that $BaFe_{12}O_{19}$ appears to be relatively insensitive to varying NaK and water volume fractions, with densities hovering around 90%. Previous work in the ZnO-NaK system showed that a change in water content of as little as 1 vol.% could significantly impact final sample density [2]. Comparing the microstructures of samples cold-sintered with 7.5 vol.% NaK and 6 vol.% H_2O (Figure 2(d)), 12 vol.% H_2O (Figure 2(e)), or 22 vol.% H_2O (Figure 2(f)) does indicate that water may cause alterations in microstructure. The sample with only 6% H_2O appears to have larger grains than the other two, while the sample with 22% H_2O has an increased presence of a secondary material coating the grains.

X-ray diffraction analysis of selected $BaFe_{12}O_{19}$ samples is presented in Figure 3. It can be seen that the hydroflux-assisted densification process introduces minimal secondary phases into the final ceramics, with small fractions of Fe_2O_3 and Na_4FeO_4 being the only secondary phases identifiable via XRD in samples cold-sintered with 5 and 7.5 vol.% NaK. The presence of Fe_2O_3 is not unexpected since preferential leaching of certain ions in materials such as $ZnFe_2O_4$ and $BaTiO_3$ has previously been noted as a challenge during the cold sintering process [1, 11]. Varying

water fractions did not have any impact on final ceramic composition. The peak at 26º indicates that the starting powder has some degree of non-stoichiometry ($Ba_{0.91}Fe_{11.68}O_{18.02}$), which persists in the densified ceramics.

Magnetic hysteresis loops for the $BaFe_{12}O_{19}$ samples are shown in Figure 4. Overall the low-temperature processed $BaFe_{12}O_{19}$ shows useful magnetic properties comparable to those of traditionally processed ceramics. Magnetization saturation values range from 64-93 emu/g and coercivities range from 1427-1789 Oe, as seen in Table 1. Values reported in the literature typically range from 40-70 emu/g for saturation magnetization and 1400-5600 Oe for coercive field [9, 13, 19, 28]. The coercivity of the cold-sintered $BaFe_{12}O_{19}$ samples is slightly lower than the literature values, however this initial study does not present optimized properties. Two key factors should be addressed to enhance magnetic performance in these samples: phase purity and powder morphology.

Deleted: ed

Deleted: d

As shown in the XRD plot in Figure 3, there is some degree of non-stoichiometry in the starting $BaFe_{12}O_{19}$ powder. This secondary non-stoichiometric phase could lead to degradation of the magnetic properties of the final ceramic [8, 28, 29]. Furthermore, the presence of small quantities of Fe_2O_3 in the final ceramics could also harm magnetic properties. The preferential leaching of barium could be circumvented by using similar techniques as Kamani et al. or Guo et al. [4, 11], i.e. performing a surface treatment on the powders prior to densification or altering the chemistry of the transport phase to pre-load it with barium ions and therefore slow the dissolution of barium from the ferrite powder.

Additionally, the starting $BaFe_{12}O_{19}$ powder had a nonideal bimodal particle size distribution with particles around 3 μm and 400 nm. Grain size can play a key role in coercive field of $BaFe_{12}O_{19}$ ceramics. Pankhurst et al. studied the magnetic properties of fine-grained (~100

nm) barium ferrite and achieved a coercivity of 5800 Oe, which is more than double that of the reference sample with 330 nm grains [29]. Mazaleyrat et al. also reported coercive fields around 5000 Oe for spark plasma sintered $BaFe_{12}O_{19}$ with grain sizes < 100 nm [9]. They referenced a commercial magnet with grain sizes >1000 nm that demonstrated a saturation magnetization similar to that of the spark plasma sintered sample, but a coercive field of only 2600 Oe. It is also pertinent to note that the spark plasma sintered samples did not achieve densities > 90%, so improved densities could further enhance magnetic properties. As previously mentioned, the low temperatures of cold sintering offer unique opportunities to control grain size and microstructure of the final ceramic, so using a finer starting powder than the one used in the presented study would allow for a nanograined ceramic that may have interesting magnetic properties.

Table 1 Processing conditions, final density, and resulting saturation magnetization and coercivity for $BaFe_{12}O_{19}$ densified via the HAD process at 300ºC for 30 minutes.

NaK (vol. %)	Water (vol.%)	Pressure (MPa)	Density (%)	M_s (emu/g)	H_c (Oe)
0	0	530	73	64	1693
5	12	530	89	--	--
5	12	1230	93	--	--
7.5	6	530	89	--	--
7.5	12	530	92	65	1693
7.5	22	530	89	64	1789
15	22	530	90	93	1427

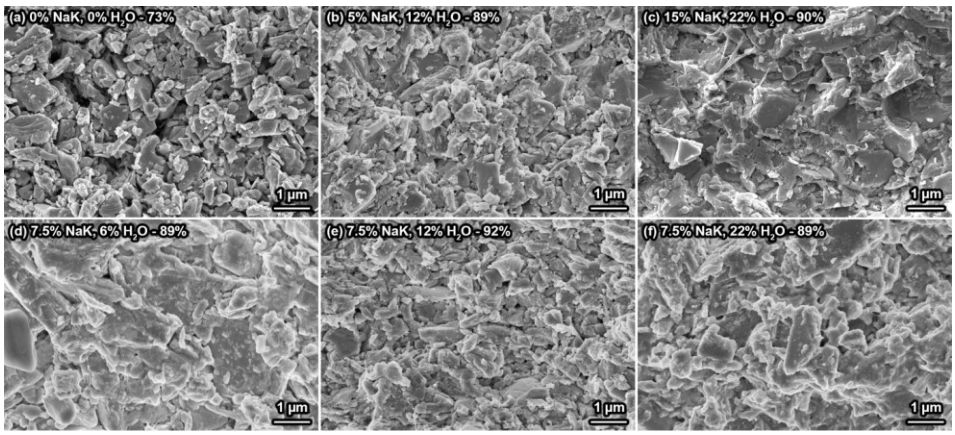

Figure 2 Representative microstructures of $BaFe_{12}O_{19}$ densified at 530 MPa and 300ºC for 30 minutes using a transport phase consisting of (a) 0% NaK and 0% H_2O, (b) 5% NaK and 12% H_2O, (c) 15% NaK and 22% H_2O, (d) 7.5% NaK and 6% H_2O, (e) 7.5% NaK and 12% H_2O, (f) 7.5% NaK and 22% H_2O. Densities are included on the images.

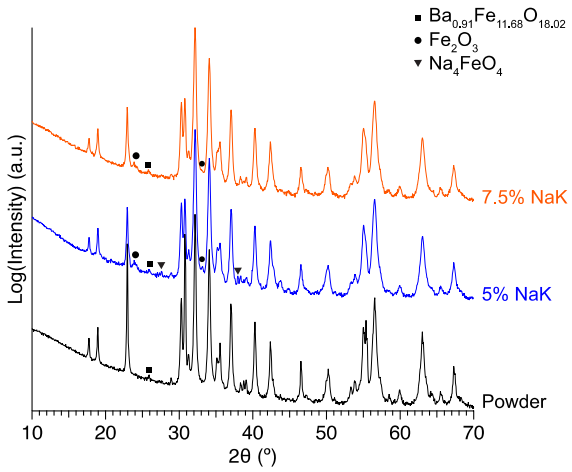

Figure 3 X-ray diffraction patterns of $BaFe_{12}O_{19}$ (a) starting powder (bottom), cold-sintered at 530 MPa and 300ºC for 30 minutes with 5 vol.% NaK and 12% H_2O (middle) and 7.5% NaK and 12% H_2O (top). The presence of a small amount of non-stoichiometric barium ferrite in the starting powder is noted.

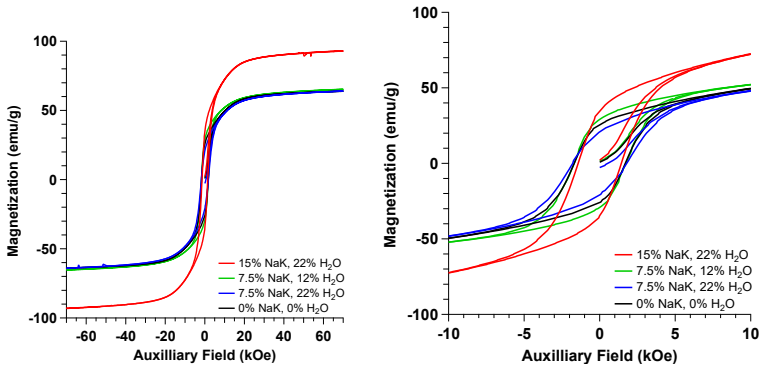

Figure 4 (a) Magnetic hysteresis loops of $BaFe_{12}O_{19}$ samples cold-sintered with varying amounts of hydroflux transport phase at 530 MPa and 300ºC for 30 minutes. (b) shows the hysteresis loops presented in (a) on a smaller scale.

IV. Conclusions

Several ferrite materials were cold-sintered at 300ºC using a hydroflux transport phase consisting of a eutectic 51:49 molar ratio of NaOH:KOH. $ZnFe_2O_4$ achieved a relative density of 96%, which is significantly higher than cold-sintered densities previously reported in the literature, while $BaFe_{12}O_{19}$ achieved densities between 89%-93%, which is the first report of $BaFe_{12}O_{19}$ being densified at such a low temperature. $NiFe_2O_4$ and $(Ni_{0.5}Zn_{0.5})Fe_2O_4$ were unable to reach densities >80% via the HAD process. Further investigation into alternative transport phases and processing conditions must be performed to realize the same success in densification in these materials as in $ZnFe_2O_4$ and $BaFe_{12}O_{19}$.

The magnetic hysteresis of cold-sintered $BaFe_{12}O_{19}$ samples was measured and the magnetization saturation and coercivity proved to be comparable to values in the literature for various processing techniques. The barium ferrite sample densified with 15 vol.% NaK and 22% H_2O had the maximum magnetization saturation of 93 emu/g and a coercivity of 1427 Oe. The

sample cold-sintered with 7.5% NaK and 22% H_2O had the maximum coercivity of 1789 Oe, but a slightly lower magnetization saturation of 64 emu/g. This work demonstrates that $BaFe_{12}O_{19}$ can be densified following the hydroflux-assisted densification approach at only 300ºC while maintaining useful magnetic properties. Future work should focus on improving the chemical nature and morphology of the starting powder to further optimize the final magnetic properties.

V. Acknowledgements

The authors would like to thank members of the Materials Characterization Laboratory and the Huck Institutes of the Life Sciences' Microscopy and Cytometry Facility at the Pennsylvania State University for use of their equipment. This material is based upon work supported by the National Science Foundation, as part of the Center for Dielectrics and Piezoelectrics under Grant Nos. IIP-1841453 and IIP-1841466. This material is based upon work supported by the National Science Foundation Graduate Research Fellowship Program under Grant No. DGE1255832. Any opinions, findings, and conclusions or recommendations expressed in this material are those of the author(s) and do not necessarily reflect the views of the National Science Foundation. Z.Q.M. acknowledges the support from the US National Science Foundation (NSF) under grant DMR 1917579.

VI. Conflicts of Interest

The authors are unaware of any conflicts of interest regarding the data and findings presented in this manuscript.

VII. References

[1] Guo H, Baker A, Guo J, and Randall CA (2016) Cold Sintering Process: A novel technique for low-temperature ceramic processing of ferroelectrics, J Am Ceram Soc 99:3489–3507.

[2] Lowum S, Floyd R, and Maria JP (2020) Hydroflux-assisted densification: applying flux crystal growth techniques to cold sintering, J Mater Sci 55:12747–12760.

[3] Grasso S, Biesuz M, Zoli L, Taveri G, et al (2020) A review of cold sintering processes, 6753:

[4] Guo H, Guo J, Baker A, and Randall CA (2016) Hydrothermal-assisted cold sintering process: A new guidance for low-temperature ceramic sintering, ACS Appl Mater Interfaces 8:20909–20915.

[5] Jing Y, Luo N, Wu S, Han K, Wang X, Miao L, and Wei Y (2018) Remarkably improved electrical conductivity of ZnO ceramics by cold sintering and post-heat-treatment, Ceram Int 44:20570–20574.

[6] Berbano SS, Guo J, Guo H, Lanagan MT, and Randall CA (2017) Cold sintering process of $Li_{1.5}Al_{0.5}Ge_{1.5}(PO_4)_3$ solid electrolyte, J Am Ceram Soc 100:2123–2135.

[7] Lowum S, Floyd R, Bermejo R, and Maria JP (2019) Mechanical strength of cold-sintered zinc oxide under biaxial bending, J Mater Sci 54:4518–4522.

[8] Sözeri H (2009) Effect of pelletization on magnetic properties of BaFe12O19, J Alloys Compd 486:809–814.

[9] Mazaleyrat F, Pasko A, Bartok A, and Lobue M (2011) Giant coercivity of dense nanostructured spark plasma sintered barium hexaferrite, J Appl Phys 109:5–8.

[10] Ndayishimiye A, Sengul MY, Sada T, Dursun S, et al (2020) Roadmap for densification in cold sintering : Chemical pathways, Open Ceram 2 2:100019.

[11] Kamani M, Yourdkhani A, Poursalehi R, and Sarraf-Mamoory R (2019) Studying the cold sintering process of zinc ferrite as an incongruent dissolution system, Int J Ceram Eng Sci 1:125–135.

[12] Funahashi S, Kobayashi E, Kimura M, Shiratsuyu K, and Randall CA (2019) Chelate complex assisted cold sintering for spinel ceramics, J Ceram Soc Japan 127:899–904.

[13] Wang HZ, He Q, Wen GH, Wang F, Ding ZH, and Yao B (2010) Study of formation mechanism of barium hexaferrite by sintering curve, J Alloys Compd 504:70–75.

[14] Mallick KK, Shepherd P, and Green RJ (2007) Dielectric properties of M-type barium hexaferrite prepared by co-precipitation, J Eur Ceram Soc 27:2045–2052.

[15] Liu Y, Li Y, Zhang H, Chen D, and Wen Q (2010) Study on magnetic properties of low temperature sintering M-Barium hexaferrites, J Appl Phys 107:10–13.

[16] Krishna KR, Kumar KV, and Ravinder D (2012) Structural and Electrical Conductivity Studies in Nickel-Zinc Ferrite, Adv Mater Phys Chem 02:185–191.

[17] Verma A, Goel TC, Mendiratta RG, and Kishan P (2000) Magnetic properties of nickel-zinc ferrites prepared by the citrate precursor method, J Magn Magn Mater 208:13–19.

[18] Yu J, Tang S, Zhai L, Shi Y, and Du Y (2009) Synthesis and magnetic properties of single-crystalline BaFe12O19 nanoparticles, Phys B Condens Matter 404:4253–4256.

[19] Zhao WY, Zhang QJ, Tang XF, Cheng H Bin, and Zhai PC (2006) Nanostructural M -type barium hexaferrite synthesized by spark plasma sintering method, J Appl Phys 99:99–102.

[20] Yang Y, Li J, Zhao J, Chen X, Gan G, Wang G, and He L (2019) Synthesis of nickel zinc ferrite ceramics on enhancing gyromagnetic properties by a novel low-temperature

sintering approach for LTCC applications, J Alloys Compd 778:8–14.

[21] Faouri SS, Mostaed A, Dean JS, Wang D, et al (2019) High quality factor cold sintered Li 2 MoO 4 –BaFe 12 O 19 composites for microwave applications, Acta Mater 166:202–207.

[22] Floyd RD (2019) Improving the Instrumentation and Science of Cold Sintering. PhD Dissertation, North Carolina State University

[23] Floyd R, Lowum S, and Maria J-P (2019) Instrumentation for automated and quantitative low temperature compaction and sintering, Rev Sci Instrum 90:

[24] Kang X (2017) Hydrothermal cold sintering. PhD Dissertation, North Carolina State University

[25] Valverde N (1988) Factors Determining the Rate of Dissolution of Metal Oxides in Acidic Aqueous Solutions, Berichte der Bunsengesellschaft für Phys Chemie 92:1072–1078.

[26] Casey WH, Banfield JF, Westrich HR, and McLaughlin L (1993) What do dissolution experiments tell us about natural weathering?, Chem Geol 105:1–15.

[27] Simpson D, Bredow T, and Gerson A (2003) Contrasting dissolution mechanisms of MgO and NiO: A quantum-chemical study. In: Uematsu K, Yokokawa H (eds) Key Engineering Materials, 253rd ed. pp 43–62

[28] An GH, Hwang TY, Kim J, Kim JB, Kang N, Jeon KW, Kang M, and Choa YH (2014) Novel method for low temperature sintering of barium hexaferrite with magnetic easy-axis alignment, J Eur Ceram Soc 34:1227–1233.

[29] Pankhurst QA, Thompson GR, Sankaranarayanan VK, and Dickson DPE (1996) Effect of ultrafine particle size and crystallinity breakdown on the ordered magnetic state in barium ferrite, J Magn Magn Mater 155:104–106.